Materials for Renewable and Sustainable Energy (2022) 11:277–286
https://doi.org/10.1007/s40243-022-00220-5

ORIGINAL PAPER

Facile fabrication, structural and electrical investigations of cadmium sulfide nanoparticles for fuel cell performance

Mervet Ramadan[1] · Mohamed S. Elnouby[2] · O. El-Shazly[1] · E. F. El-Wahidy[1] · A. A. M. Farag[3] · N. Roushdy[4]

Received: 2 October 2022 / Accepted: 17 November 2022 / Published online: 12 December 2022

Abstract

In the present work, CdS nanoparticles were synthesized and analyzed for use in fuel cell applications. The X-ray diffraction investigation showed that CdS possesses a cubic polycrystalline structure. For the (111) plane, the average values of mean crystallite size, microstrain, and dislocation density were calculated and found to be 1.935 nm, 0.0758, and 0.267 nm^{-2}. The average crystallite size was additionally calculated and found to be 2.02 nm using the modified Scherrer's plot. The observed blue shift in the photoluminescence of CdS is caused by the quantum size impact of the nanocrystalline structure. A broad emission band at 590 nm is produced by the recombination of a hole in the valence band of CdS with an electron confined in a sulfur vacancy. The average Cd/S ratio is good and comparable, according to the EDS analysis, which is close to the theoretical values and almost exactly fits the ideal structure. A thermogravimetry diagram was used to establish the thermal stability of CdS across a wide range of temperatures. Fuel cell application features peaks were investigated by the cyclic voltammetry of CdS under various conditions. The linear sweep voltammetry was used to analyze the electrochemical performance of CdS electrodes in fuel cells. Electrochemical impedance spectroscopy (EIS) was also used and the results confirmed that nickel substrate is regarded as being superior to stainless steel in terms of performance.

Keywords Nanoparticles · Fuel cell · Liner sweep voltammetry · Electrochemical impedance spectroscopy

Introduction

Nanoparticles of CdS have attracted a lot of attention due to their unique size-dependent chemical and physical properties. The production of different CdS nanostructures has been the subject of extensive study [1, 2]. Green oktite is the crystalline form of cadmium sulfide that is found in nature. The substance is commonly utilized in paint pigments as well as baked enamels, ceramics, and plastics. With good color retention and resilience to alkalis, it gives maroon a bright yellow tint [1]. In addition to having a direct band gap of 2.42 eV and great stability, CdS also possesses a compact crystallographic cell structure, minimal absorption loss, and electronic affinity.

The structural, optical, electrical, magnetic, and dielectric properties of CdS make it a very fascinating material. Its optoelectronic and photoconductive properties make it an even more fascinating substance [3]. The two primary structural kinds of CdS are polytypes of wurtzite and zinc blende. The crystal structure of CdS is wurtzite-like and hexagonal. Cubic zinc blende structures are present in CdS nanocrystallites [4].

A significant increase in the binding energy occurs when the crystallite radius approaches or falls below the Bohr exciton radius, and this significant change at the nanoscale has drawn a lot of interest to nanocrystalline CdS in recent years. Due to its widespread application in devices like field effect transistors, light-emitting diodes,

✉ Mohamed S. Elnouby
m_nano2050@yahoo.com

1 Physics Department, Faculty of Science, Alexandria University, Alexandria, Egypt

2 Composite and Nanostructured Materials Research Department, Advanced Technology and New Materials Research Institute, City of Scientific Research and Technological Applications (SRTA-City), New Borg El-Arab, Alexandria 21934, Egypt

3 Thin Film Laboratory, Physics Department, Faculty of Education, Ain Shams University, Heliopolis 11757, Roxy, Cairo, Egypt

4 Electronic Materials Department, Advanced Technology and New Material Institute, City of Scientific Research and Technology Applications, New Borg El Arab City, Alexandria 21934, Egypt

photocatalysis, and biological sensors, CdS nanoparticles are by far the most studied system among all semi-conducting nanoparticles. In addition, when exposed to light, CdS conductivity rises (leading to uses as photoresistors). Both phosphorescence and cathodoluminescence are common characteristics of CdS. A solid-state laser made of solid CdS is possible. Synthetic cadmium pigments are prized for their great opacity, excellent chemical resistance, strong thermal stability, and light- and weather-fastness. Sulfate-reducing bacteria naturally create cadmium sulfide, which is being studied as a possible method of manufacturing nanocrystalline cadmium sulfide. Cadmium sulfide is utilized in solar cells, photodetectors, lasers, and light-emitting diodes, among other devices. CdS nanoparticles are promising candidates for optoelectronic applications. However, CdS is an unstable substance that readily transforms into other substances when heated in the air [4].

In order to understand how charge transfer and electrocatalysis function in the generated nanoparticles, electrochemical techniques such as cyclic voltammetry and impedance spectroscopy are applied. This study claims that adding CdS nanoparticles to electrodes improves their properties compared to bare electrodes. Furthermore, this study is required to confirm the beneficial uses of the produced CdS nanoparticles, particularly in the area of fuel cell applications.

In the current work, a potential synthesis of CdS nanostructures has been carried out employing thiourea ($CS(NH_2)_2$) as a source of sulfur ions (S^{-2}) and cadmium chloride ($Cd(CH_3COO)_2$ as a source of cadmium ions (Cd^{+2}). X-ray diffraction, high-resolution transmission electron microscopy techniques, and energy dispersive spectroscopy (EDS) were used in the thorough structural and compositional research. At various cyclic voltammetry electrochemical deposition scanning rates, distinct micromorphologies of electrode materials were observed. A cyclic voltammogram for steel and nickel materials with various saturated electrolytes and electrodes was considered. Using linear sweep voltammetry, the electrochemical performance of CdS electrodes in fuel cells was evaluated. In addition, electrochemical impedance spectroscopy was also investigated.

Experimental methods

Synthesis of CdS

Using a well-mixed powder of $Cd(CH_3COO)_2.2H_2O$ and Thiourea that was acquired from Sigma Aldrich, a ball mill technique was used to create cadmium sulfides. In the furnace, the mixture was heated to 200 °C for 2 h of sintering.

Structural characterizations

Scanning electron microscopy, using JEOL, JSM-6360 LA- Japan was used for the investigation of the surface morphology and homogeneity of the prepared CdS samples. The energy dispersive X-ray (EDX), high-resolution transmission electron microscopy at an accelerating voltage of 200 kV (JEOL, TEM-2100 plus, Japan), and the microstructure of CdS were also investigated. The powder PL analysis was calculated using transmittance spectra and photoluminescence (PL) emission spectra. The particle size was assessed using a Particle Size Analyzer (PSA) (LS55 Luminescence Spectrometer, Perkin Elmer).

Electrode preparation and electrochemical measurements

A mix of 20 mg of fabricated cadmium sulfide (CdS) with 10 mg graphite, 10 mg PVDF, and 2 ml (DMF) solution to prepare the ink was used. To prepare the electrode ink, the liquid was sonicated for 15 min at room temperature. After which, the surface of the (10 × 10 mm) stainless steel substrate was treated with a drop of the prepared ink, and the prepared electrodes were dried at 65 °C overnight.

Electrochemical calculations

Cyclic voltammetry measurements on CdS were carried out to investigate various electrochemical properties that were present. All investigations were conducted at room temperature using a working electrode with a 1 cm^2 surface area. By quantitatively looking into the relationship between i_p and v, such as in the diffusion-controlled battery-behavior mode, we may determine the mode of transport processes according to the anodic and cathodic peak current (i_p (A)) scan rates (1 V/s). Thus, according to the following equation, in the case of the former, a diffusion-controlled reaction, i_p is proportional to $V^{1/2}$.

$$i_p = \left(2.69 \times 10^5\right) n^{3/2} A D^{1/2} v^{1/2} C^*, \quad (1)$$

where i_p, n, A, D, v, and C^* represent the peak current (i_p A), the number of electrons transferred, the area of the electrode (A, cm^2), the diffusion coefficient (D, cm^{-1}), the scan rate (v, $V\ s^{-1}$) and the bulk concentration of analyte (C^*, mol cm^{-3}), respectively [5].

Results and discussions

X-ray diffraction analysis of CdS

Figure 1A depicts the XRD patterns of CdS nanoparticles. The great variety of unique sharp crystalline peaks that appear in each diffraction pattern attests to the manufactured samples' polycrystalline character. The outcomes agree with the cubic CdS system reference pattern (JCPDS No. 00-042-1411) [6]. The optimum orientations of CdS were determined to be (111), (220), (311), and (400). Low intensities and broad half-peaks characterize the extra peaks that the XRD scan may reveal. The cubic system of the CdS sample, which is nearly polycrystalline and nanocrystalline in nature, displays exceptional crystallinity.

Some important microstructural characteristics may be calculated using the right formulae by examining the XRD patterns. By analyzing the XRD patterns, certain significant microstructural parameters may be computed using Scherrer's formulae. The extended X-ray diffraction line is also influenced by important parameters including internal crystallite size, D, microstrain, and dislocation density, it has been highlighted [6–8]. The average values of D may be computed using the following equation [7, 8]:

$$D = \frac{K\lambda}{\beta \cos\theta}, \tag{2}$$

where $\lambda = 0.1542$ nm is the Cu-K_α wavelength, K is a constant, and β is the FWHM, and the microstrain, ε can be expressed as follows:

$$\varepsilon = \frac{\beta}{4\tan\theta}. \tag{3}$$

And the dislocation density can be obtained using the following:

$$\delta = \frac{1}{D^2}. \tag{4}$$

The computational results for the mean crystallite size, D, the microstrain, and the dislocation density, are presented in Table 1 and Fig. 1b. The lower magnitude of the microstrain indicates that there are likely fewer lattice defects existent since the line diffraction width has most likely diminished [7].

The basis for the modified Scherrer formula is that, in order to achieve the average value of D through all of the desired orientation peaks, mistakes must be mathematically reduced using the least squares method [8]. It is possible to rewrite the basic Scherrer formula as follows:

$$\beta = \frac{K\lambda}{D\cos\theta} = \frac{K\lambda}{D}.\frac{1}{\cos\theta}. \tag{5}$$

Make a logarithm here on both sides.

$$\ln\beta = \ln\frac{K\lambda}{D\cos\theta} = \ln\frac{K\lambda}{D} + \ln\frac{1}{\cos\theta}. \tag{6}$$

If the results of ln against ln(1/cosθ) are given, a straight line with a slope of nearly one and an intercept of roughly lnβ/L must be drawn. The experimental straight line must have a 45° slope since tan 45 = 1, Fig. 1b. However, the least squares approach offers the best slope and the most accurate lnK/L since errors are connected to experimental data. The intercept is then computed, and a single value of D is determined to be 2.02 nm.

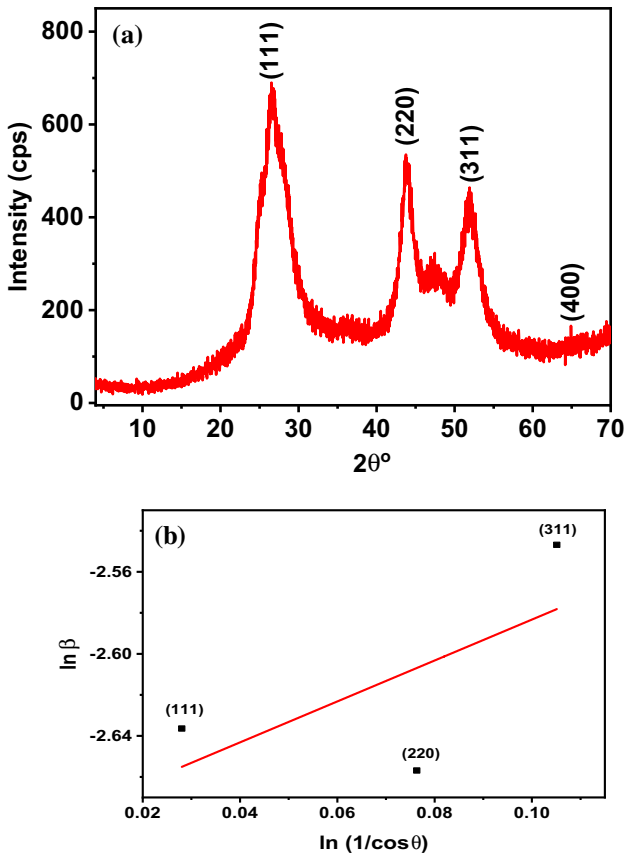

Fig. 1 Plot of **a** The X-ray diffraction pattern, and **b** lnβ vs. ln (1/cosθ) of CdS sample

Table 1 XRD parameters of CdS

Plane	β	D(nm)	ε	δ(nm^{-2})
(111)	0.071616	1.935	0.0758	0.267
(220)	0.070166	2.132	0.0436	0.220
(311)	0.07832	1.965	0.0402	0.259

Particle size analysis

Using the N5 Submicron Particle Size Analyzer, it was possible to calculate the average particle size. On the dynamic light scattering theory, the investigation is built. The particle size was revealed to be between 5 nm and 5 µm. The detecting system has different scattering angles, and the average particle size measured by low-angle scattering is found to be 65 nm, while the value obtained by higher-angle scattering is determined to be 850 nm, as seen in Fig. 2. The low-angle scattering of CdS reveals the properties of nanostructures that have several applications in a variety of fields. The utilization of nanoscale particles in artificial implant manufacturing systems is receiving a lot of attention. Both in vitro and in vivo qualities are influenced by the nanosized particles. In addition, these nanoparticles displayed excellent biocompatibility and biodegradability characteristics, supporting the regeneration of bone and other uses[9].

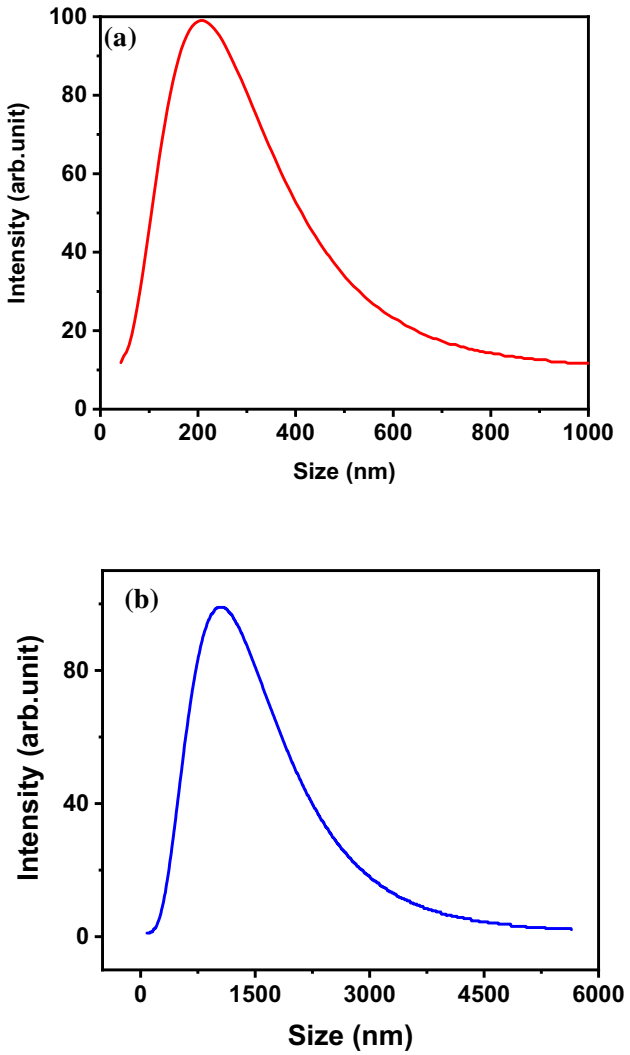

Fig. 2 Plot of particle size distribution **a** at low angle scattering, and **b** high angle scattering of the prepared CdS

Morphological characteristics of CdS

Using electron microscopy, the surface morphology of cadmium sulfide nanoparticles was studied. The surface morphology of CdS sample surfaces as determined by SEM images of various magnifications is provided in Fig. 3a–d. The images display several inhomogeneous structures that are unequally distributed and dense. Every micrograph entirely covers the surfaces of CdS. The substance is highly dense, devoid of cracks, and commonly irregular in shape. The average grain size was discovered using image analysis tools. Following the completion of the grain size statistical distribution, Fig. 3e displays the grain size distribution through the surface. The major section of the grain size looks to be around 65 nm, or around the largest fraction of the grain size in nanometers. The surface roughness variation over the examined region of the produced CdS is shown in Fig. 3f. The figure also displays the relative height of the surface roughness, which was determined to be between 40 and 50 nm. The samples' estimated average particle sizes are bigger than the predicted crystallite size based on X-ray diffraction examination. This is because X-rays can only see the well-ordered portions of crystallites; they cannot see the disordered grain boundaries, which take up a significant amount of space, and there is a chance that multiple crystallites could accumulate and form an aggregation of particles in the solution even after being exposed to ultrasonic waves [10].

Structural characteristics using HR-TEM of CdS

Transmission electron microscopy images of CdS are shown in Fig. 4a–d, which clearly illustrate the crystalline features. The most conventional size of CdS nanoparticles, which are shown to be grouped together with extremely small particles in most places and various directions. Furthermore, there are not any surface pinholes. In accordance with those interpreted from XRD, the SAED pattern in Fig. 4e displays three diffraction rings that closely correspond to the (111), (220), (311), and (400) crystal planes of the cubic CdS. Figure 4f reveals the elemental composition of cadmium sulfide that was investigated using energy dispersive X-ray spectroscopy (EDS). The results of the compositional analysis by EDS are displayed in Table 2. The average Cd/S ratio is good and comparable to those described in the literature [11] in terms of both atomic and weight percentages, according to the EDS results, which demonstrate that Cd and S elements are present in the synthesized structure. The Cd/S atomic ratios in the samples are also 1/1.102, which is quite near

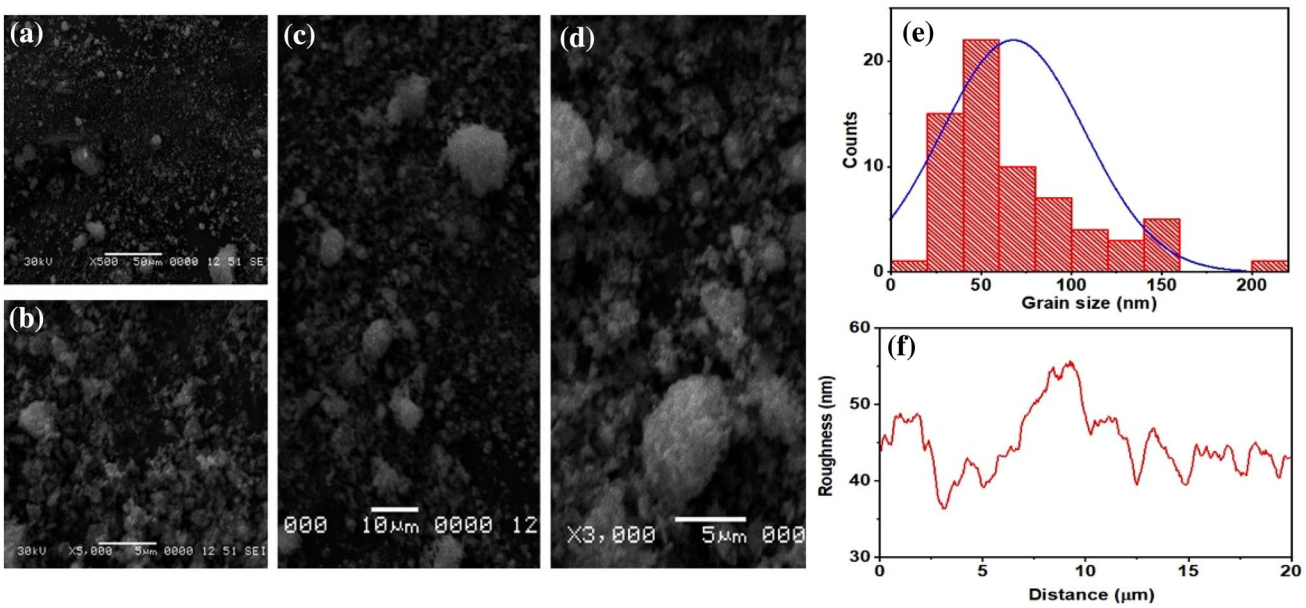

Fig. 3 **a**–**d** SEM analysis of CdS, **e** Grain size distribution, and **f** roughness pattern

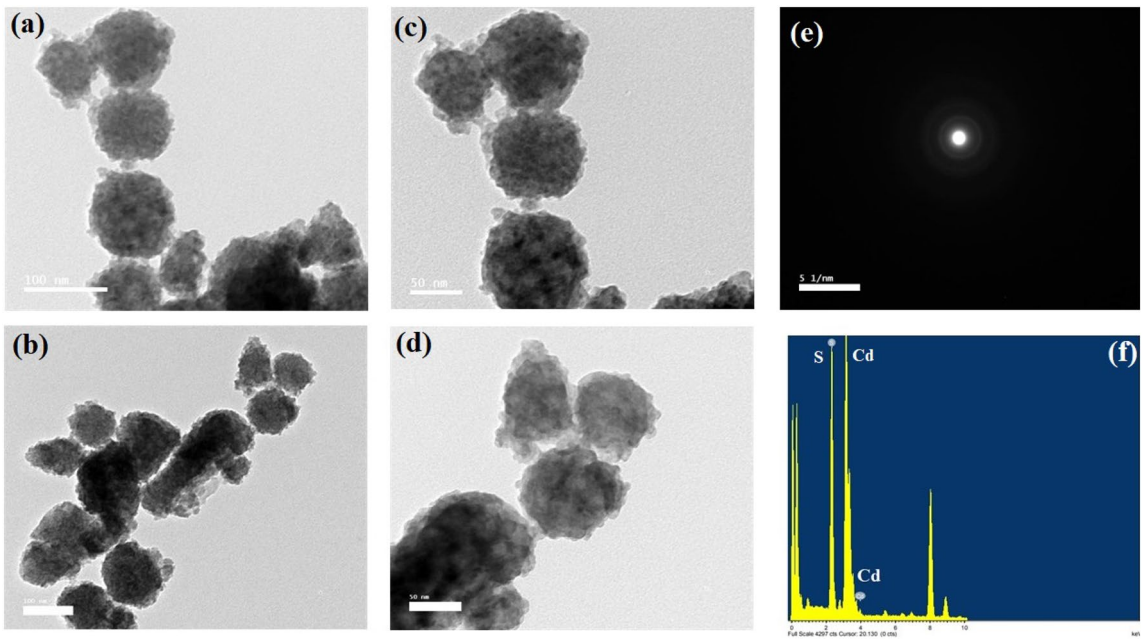

Fig. 4 **a**–**d** TEM micrograph at different magnifications, **e** SAED of the prepared CdS, and **f** EDS diagram of the prepared CdS

Table 2 Elemental composition analysis of prepared CdS nanoparticles

Element	Peak area	Area sigma	K factor	Weight%	Atomic%
S K	46,248	420	0.959	20.56	47.57
Cd K	95,043	855	1.803	79.44	52.43
Totals				100%	100%

to the theoretical values and almost precisely fits the ideal structure [12].

Using high-resolution transmission electron microscopy, the crystalline structure and its identifying features of the CdS nanostructure may be provided (HR-TEM). The HR-TEM picture of CdS nanoparticles at various magnifications is shown in Fig. 5a, b. The structure does not have a

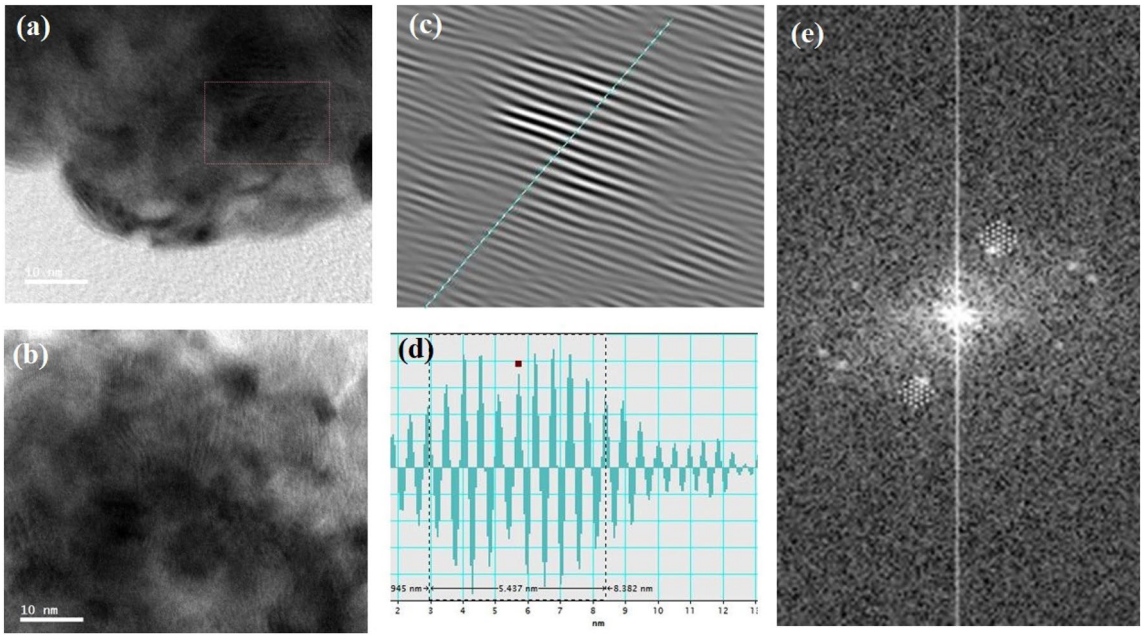

Fig. 5 **a**, **b** HR-TEM micrograph of prepared CdS, **c** Fourier filtered image of the planes, **d** FFT spectrum of ZnS, **e** FFT image of CdS

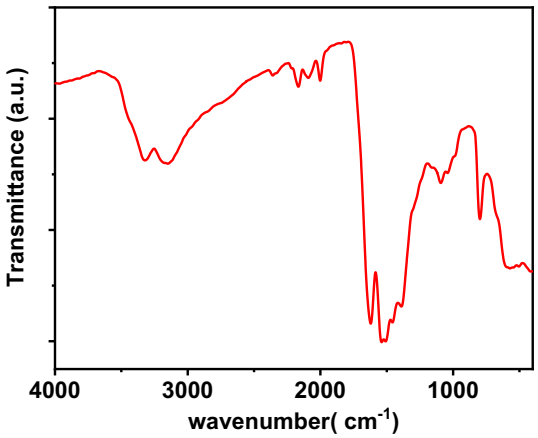

Fig. 6 FTIR spectrum of CdS sample

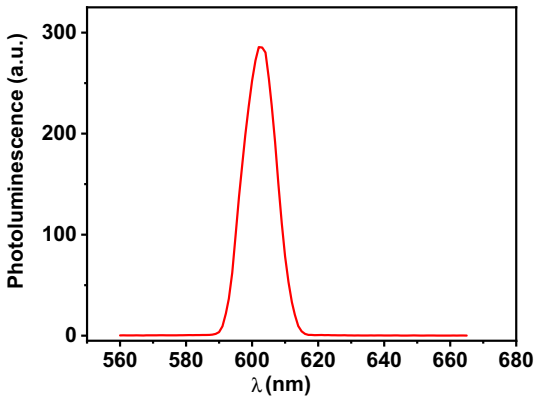

Fig. 7 Spectral dependence of PL of prepared CdS

particular crystalline shape; however, there are a few crystal planes that may be examined under high-resolution settings. Fourier-filtered images (Fig. 5c) show the preferred planes of CdS. The lattice fringe d-spacing measurements of 0.335 nm can be detected, and the corresponding Fast Fourier Transform (FFT) image is displayed in Fig. 5d, e that demonstrates the (111) crystal plane of the cubic CdS.

FT-IR spectral analysis of CdS

The FTIR spectrum of a manufactured CdS, which ranged from 400 to 4000 cm^{-1}, is depicted in Fig. 6. To detect functional groups in molecules and assess if synthesis occurred, FTIR analysis is a useful method. The specific bands in the spectrum that were shown to be around 550 cm^{-1} match typical CdS vibration modes as confirmed by Ubale et al. [13]. The bands at around 1520 and 1320 cm^{-1} are caused by the CH group's bending and the CS group's stretching modes, respectively. At 1650 cm^{-1}, the band resulting from the NH's bending was apparent. The adsorbed water molecule during synthesis is shown as a wide band by the band at 3331 cm^{-1} [14] and then the production of CdS nanocrystals is well supported by these observations [15].

Photoluminescence characteristics of CdS

Figure 7 displays the PL spectra at a 350 nm excitation wavelength. As already mentioned, the produced CdS exhibits a clearly blue-shifted beginning of emission in comparison to the bulk CdS particles. The quantum size effect of nanocrystalline CdS is responsible for the noticeable blue shift in these samples. The recombination of a hole in the valence band of CdS with an electron trapped in a sulfur vacancy results in a wide emission band at 590 nm, which is visible in the PL spectrum [16]. The findings are in line with those for CdS reported by Firooz et al. [16] and Chae et al. [17].

Thermogravimetric analysis (TGA) of CdS

Using TGA analysis, the thermal stability of the produced CdS sample was examined with heating from room temperature to 1100 °C in a nitrogen atmosphere at a rate of 10 °C/min. The results are shown in Fig. 8. According to Fig. 8, the thermal degradation of CdS occurs in five phases, with the first stage occurring between 30 and 250 °C, the second between 250 and 350 °C, the third between 350 and 650, the fourth between 650 and 730, and the fifth between 730 and 970 °C. Losses of 0.9214%, 2.225%, 5.730%, 11.790%, 8.13%, and 71.59% were discovered. The first weight loss at 61.66 °C was caused by loss of physisorbed moisture [18]. The CdS started to degrade at 639.75.09 °C, which caused a significant weight loss. This was followed by another loss of weight at 725.00 °C, and then another loss of weight owing to the structural breakdown of CdS at 962.09 °C. The findings supported the idea that CdS displays thermal stability for a variety of applications. The results are consistent with what has been published for CdS by Banizi and Seifi [19]. The results for thermal stability of the prepared CdS indicate high thermal stability compared with those published by Banizi and Seifi [19], Jassim et al. [20], and Smirnov et al. [21].

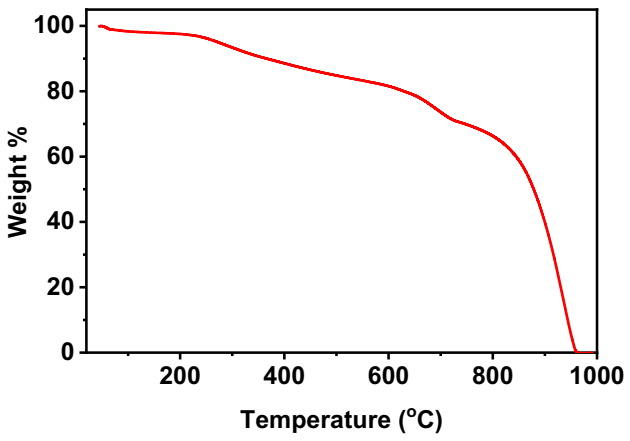

Fig. 8 Plot of thermal gravimetric analysis, TGA of the prepared CdS sample

Cyclic voltammetry of CdS

A well-known method for measuring the electrochemically active surface area of a catalyst in an electrode through adsorption/desorption cycles is cyclic voltammetry. The cyclic voltammogram for CdS electrodes in various saturated electrolytes is shown in Fig. 9a. The scan rate was set at 100 mV/s and the potential was modified from − 1 to 1 V. The anodic peaks for nickel material were obtained at 0.53 V and 0.25 V, respectively, for steel substance (Fig. 9b). The decrease in Cd behavior is shown by the cathodic peaks. Following is a representation of the cathodic and anodic reactions [22, 23].

$$Cd^{+2} + 2e^{-} \rightarrow Cd, \tag{7}$$

$$Cd \rightarrow Cd^{+2} + 2e^{-}. \tag{8}$$

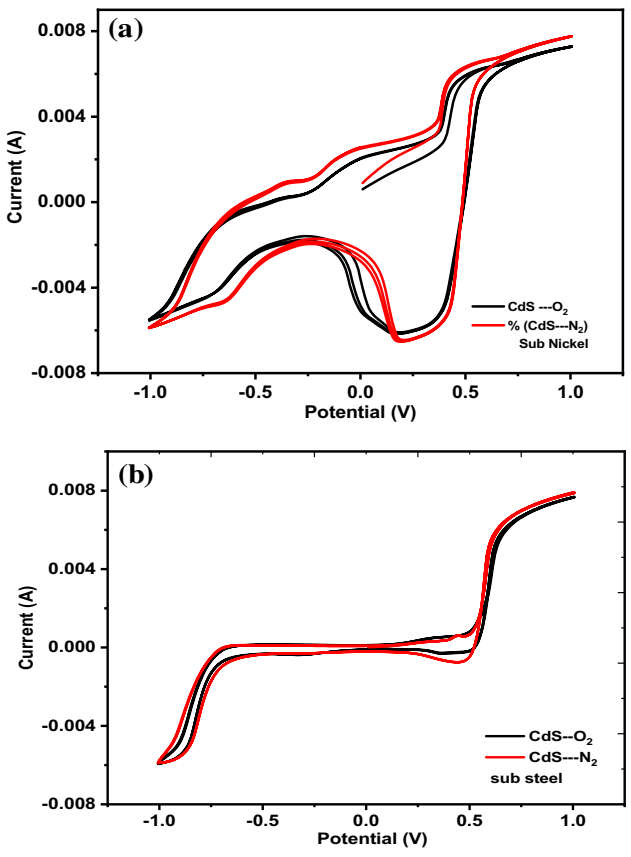

Fig. 9 **a** and **b** Cyclic voltammogram for different electrodes and different saturated electrolytes, **a** for steel substrate and **b** for nickel substrate

Electrochemical impedance spectroscopy (EIS)

Because it is non-destructive and offers some helpful data regarding fuel cell performance, Electrochemical Impedance Spectroscopy (EIS) is a strong diagnostic testing approach for fuel cells. The EIS analysis is demonstrated in Fig. 10a and b. Figure 10a shows the impedance for the CdS@SS electrode, while Fig. 10b displays the CdS@Ni electrode for the Nyquist plot of EIS measurements of CdS electrodes in the electrolyte (KOH) in a frequency range of 100 kHz to 0.1 Hz. With a depressed semi-circle in the high-frequency band, all of the samples exhibit almost the same electrolyte resistance (R_S) values. With a depressed semi-circle in the high-frequency band, all the samples exhibit almost the same electrolyte resistance (R_S) values. The parallel combination of the charge transfer resistance (RCT) of the electrochemical process is blamed for the depressed semi-circle plot's existence. According to the following Eq. (9), the system's impedance (Z) is determined from its resistance (R_s), capacitance (Cdl), and applied frequency (f) under an alternating sinusoidal potential [24].

$$Z = \frac{iR_{cT}}{1 - \omega R_{cT}}, \tag{9}$$

where i is the exchange current density of the redox reaction. The produced CdS-better electrode's electrochemical behavior and electrical characteristics were demonstrated by the electrochemical impedance spectroscopy's (EIS) significantly reduced charge transfer resistance. Depending on measurements and estimations related to electrochemistry, nickel substrate performs better than stainless steel according to its I_p and diffusion coefficient as listed in Table 3.

Conclusions

In conclusion, utilizing cadmium acetate and thiourea as starting reactants, we created CdS nanorods. This approach is easy and inexpensive. Several strategies had been used effectively to produce and examine CdS nanoparticles. The produced CdS nanoparticles were of the cubic phase, as evidenced by the X-ray diffraction pattern. The development

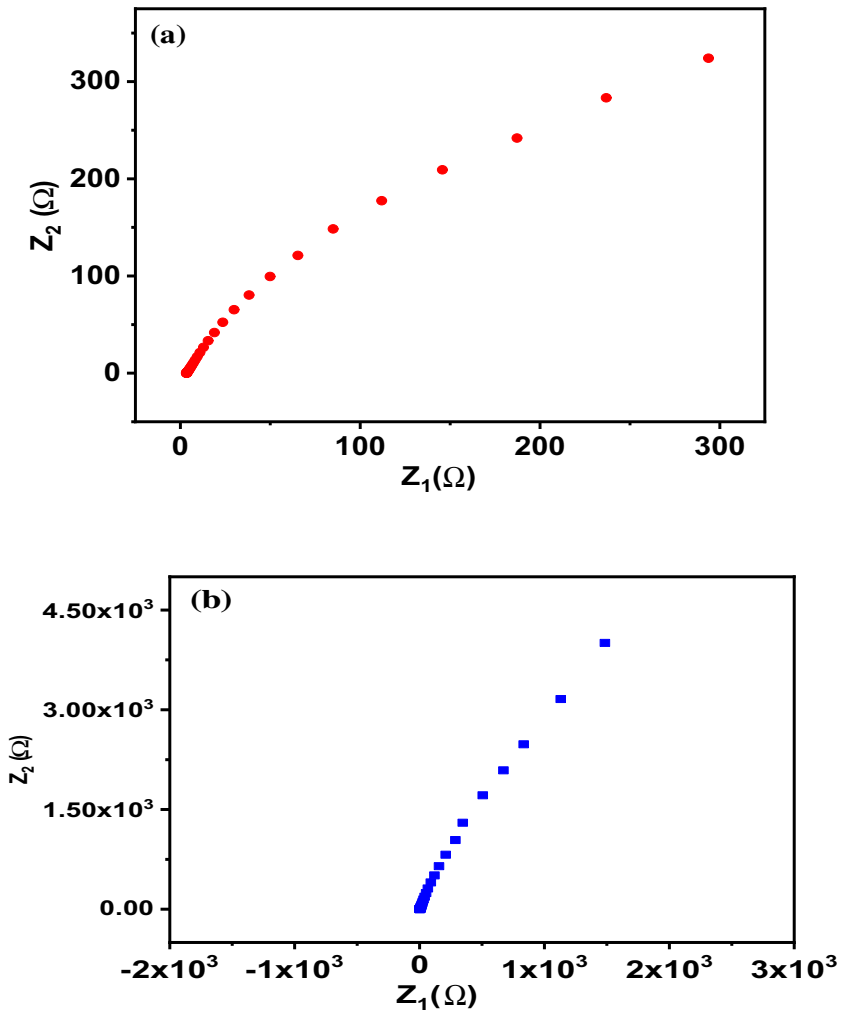

Fig. 10 **a** FRA impedance for CdS@SS electrode and **b** FRA impedance for CdS@Ni electrode

Table 3 Electrochemical characteristics of CdS-based electrodes

Electrode	Electorate	Substrate	i_p is the peak current(A)	D is the diffusion coefficient of the species
CdS steel sub	0.5 KOH –O_2	Steel	2.4843×10^{-4}	0.00341×10^{-14} cm^{-2} s^{-1}
CdS steel sub	0.5 KOH –N_2	Steel	7.907×10^{-4}	0.03467×10^{-14} cm^{2} s^{-1}
CdS Ni sub	0.5 KOH –O_2	Nickel	0.00604	2.02×10^{-14} cm^{-2} s^{-1}
CdS Ni sub	0.5 KOH –N_2	Nickel	0.006516	2.35×10^{-14} cm^{-2} s^{-1}

of the CdS nanostructure was seen using the FT-IR spectra. Results from HR-TEM confirmed that these nanostructures were constrained in size. The recombination of a hole in the valence band of CdS with an electron contained in a sulfur vacancy results in a wide emission band at 590 nm. Liner sweep voltammetry was used to assess the electrochemical performance of CdS electrodes in fuel cells.

Acknowledgements The authors would like to express their appreciation to the Physics Department, Faculty of Science, Alexandria University, and Physics Department, Faculty of Education, Ain Shams University, as well as the Electronics Materials Department, Advanced Technology and New Materials Research Institute, City of Scientific Research and Technological Applications (SRTA-City), for providing the facilities for carrying out this research.

Funding Open access funding provided by The Science, Technology & Innovation Funding Authority (STDF) in cooperation with The Egyptian Knowledge Bank (EKB).

Data availability All data generated or analysed during this study are included in this published article.

References

1. Devamani, R.H.P., Kiruthika, R., Mahadevi, P., Sagithapriya, S.: Synthesis and characterization of cadmium sulfide nanoparticles. Int. J. Innov. Sci. Eng. Tech. **4**, 2348–7968 (2017)
2. Islam, S., Hasan, T.H., Mohammad, S., Rashid, J.: A systematic study on chemically deposited cadmium sulfde (CdS) thin film. J. Theor. Appl. Phys. **14**, 265–274 (2020)
3. F.Yaying .Transition Metal Chalcogenide (Cadmium Sulfide) Nanoparticles: (Bio)synthesis, Characterization andPhotoelectrochemical Performance Duke University ProQuest Dissertations Publishing, 2019, 27545101.
4. Kashuba, A.I., Andriyevsky, B., Semkiv, I.V., Ilchuk, H.A., Petrus, R.Y., Shyshkovskyi, S.V.: Calculation of the vibrational spectra of CdSe and CdS crystals with zinc blende structure. Mater. Proc. **62**, 5812–5818 (2022)
5. Sürücü, Ö.: Electrodeposition of cadmium sulfide and lead (II) Sulfide onto polycrystalline gold electrode. J. Biol. Chem. **48**, 125–135 (2020)
6. Habibi, M.H., Rahmati, M.H.: Fabrication and characterization of ZnO@CdS core–shell nanostructure using acetate precursors: XRD, FESEM, DRS, FTIR studies and effects of cadmium ion concentration on band gap. Spectrochimica Acta Part A: Mol. Biomol. Spectrosc. **133**, 13–18 (2014)
7. Hassanien, A.S., Akl, A.A.: Microstructure and crystal imperfections of nano-crystalline sprayed iridium oxides thin films. Phys. B **473**, 11–19 (2015)
8. Iranifam, M., Dadashi, Z.: Chemiluminescence determination of vancomycin by using CdS nanoparticles–luminol–O_2 system, Spectroch. Acta Part A: Mol. Biomol. Spectrosc. **267**, 120489 (2022)
9. Murugan, S.S., Anil, S., Venkatesan, J.: Polysaccharide nanoparticles. Micro Nano Technol. **22**, 603–614 (2022)
10. Saafan, S.A., Assar, S.T., Moharram, B.M., El Nimr, M.K.: Comparison study of some structural and magnetic properties of nano-structured and bulk Li-Ni-Zn ferrite samplesJ. Magn. Magn. Mater. **322**, 628–632 (2010)
11. Kakhaki, Z.M., Youzbashi, A.A., Sangpour, P., Naderi, N., Orooji, Y.: Influence of Cd salt concentration on the photoconductivity of CdS thin films prepared by chemical bath technique. Mater. Sci. Semicond. Proc. **148**, 106773 (2022)
12. Balavijayalakshmi, J., Sonia, D.: Impact of iron doping on structural and optical properties of cadmium sulphide nanoparticles. Mater. Today Proc. **50**, 117–122 (2022)
13. Ubale, A.U., Chipade, K.S., Bhute, M.V., Raut, P.P., Malpe, G.P., Sakhare, Y.S., Belkhedkar, M.R.: Structural, optical and electrical properties of nanostructured CdS:CuS composite thin films grown by CBD method. Inter. J. Mater. Chem. **2**, 165–172 (2012)
14. Erturk, K., Isik, S., Aras, O., Kaya, Y.: Investigation of structural, spectral, optical and nonlinear optical properties of nanocrystal CdS: electrodeposition and quantum mechanical studie. Optik **243**, 167469 (2021)
15. Li, R., Li, Y., Feng, W., Wu, H.W., Zhong, X., Yongjun, M., Xie, R.: Facile synthesis, optical properties regulation and boosted photocatalytic degradation performance for organic pollutants of Mn:$CuInS_2$/CdS nanocrystals. J. Luminescence **252**, 119355 (2022)
16. Firooz, A.A., Mahjoub, A.R., Ziba, R.D.: Synthesis, characterization and PL properties of Cds nanoparticles confined within a functionalized SBA-15 Mesoprous, World Academy of Science. Eng. Technol. **5**, 128–130 (2011)
17. Chae, W.-S., Ko, J.-H., Hwang, I.-W., Kim, Y.-R.: Emission characteristics of CdS nanoparticles induced by confinement within MCM-41 nanotubes. Chem. Phys. Lett. **365**, 49–56 (2002)
18. Sambathkumar, C., Ranjithkumar, R., Ezhil Arasi, S., Manikandan, A., Nallamuthu, N., Krishna Kumar, M., Arivarasan, A., Devendran, P.: High-performance nickel sulfide modified electrode material from single-source precursor for energy storage

application. J. Mater. Sci.: Mater. Electron. **32**, 20058–20070 (2021)
19. Banizi, Z.T., Seifi, M.: Optical properties of hydrothermally synthesized TGA-capped CdS nanoparticles: controlling crystalline size and phase. Mater. Res. Express **4**, 105007 (2017)
20. Smirnov, M.S., Buganov, O.V., Tikhomirov, S.A., Ovchinnikov, O.V.: Femtosecond dynamics of photoexcitation in hybrid systems of CdS quantum dots with methylene blue. Phys. E. **118**, 113898 (2020)
21. Jassim, S., Abbas, A., AL-Shakban, M., Ahmed, L.: Chemical vapour deposition of CdS thin films at low temperatures from cadmium Ethyl Xanthate Egypt. J. Chem. **64**, 2533–2538 (2021)
22. Kim, S.H., Han, W., Lee, J.: Electrochemical characterization of CdSe and CdTe thin films using cyclic voltammetry. Curr. Appl. Phys. **10**, S481–S483 (2010)
23. Salaria, K., Mehta, N., Krishna, C., Mehta, S.K.: Electrochemical detection of TNT using CdS nanoparticles via cyclic voltammetry and amperometry. Curr. Res. Green Sust. Chem. **4**, 100166 (2021)
24. Ameen, S., Shaheer Akhtar, M., Soon Kim, Y., Shin, H.-S.: Synthesis and electrochemical impedance properties of CdS nanoparticles decorated polyaniline nanorods. Chem. Eng. J. **181–182**, 806–812 (2012)